EXAFS DETERMINATION OF THE CHANGE IN THE STRUCTURE OF RHODIUM IN HIGHLY DISPERSED $Rh/\gamma\text{-}Al_2O_3$ CATALYSTS AFTER CO AND/OR H_2 ADSORPTION AT DIFFERENT TEMPERATURES

H. F. J. VAN'T BLIK*, J. B. A. D. VAN ZON, D. C. KONINGSBERGER and R. PRINS

Laboratory for Inorganic Chemistry, Eindhoven University of Technology, P.O. Box 513, 5600 MB Eindhoven (The Netherlands)

Summary

Extended X-ray absorption spectroscopy (EXAFS) has been applied to study the Rh K-edge of two ultradisperse Rh/Al_2O_3 catalysts containing 0.47 and 1.04 wt.% rhodium respectively. The structural properties of the Rh crystallites were determined after reduction with H_2, evacuation at elevated temperatures, CO admission at room temperature, CO desorption, CO admission at 523 K (at which temperature the Boudouard reaction takes place) and after hydrogenation of CO at 523 K.

During reduction of the catalyst, metallic rhodium crystallites are formed which are attached to the support via Rh^0—O^{2-} bonds, implying zero-valent rhodium. The Rh—Rh nearest-neighbour distance in the particles is contracted to 2.63 Å in vacuum and relaxes to 2.68 Å (similar to the bulk value) upon hydrogen chemisorption. Adsorption of CO at room temperature onto the reduced catalysts results in a partial disruption of the small Rh crystallites, ultimately leading to rhodium geminal dicarbonyl species. A subsequent desorption of CO leads to rearrangement of the metal clusters. The oxidation state of rhodium alters from 0 to 1+ upon CO chemisorption, and becomes 0 again after CO desorption. After CO admission at 523 K, the rhodium particles break up completely, probably because of intercalation of carbon and/or oxygen atoms. The highly dispersed Rh/Al_2O_3 catalysts change to poorly dispersed systems after reaction between CO and H_2 at 523 K, due to sintering of the metallic crystallites.

Introduction

Knowledge of the structure and oxidation state of rhodium in highly dispersed rhodium catalysts is important for an understanding of its catalytic selectivity and activity. For instance, there are indications that the

*Author to whom correspondence should be addressed.

0304-5102/84/$3.00

hydrogenation of carbon monoxide yields oxygen-containing products such as methanol and ethanol when rhodium ions are present [1, 2].

Many characterization studies performed on ultradispersed rhodium supported catalysts have been reported in which a diversity of techniques has been used [3 - 10].

The CO infrared spectrum between 1800 and 2100 cm^{-1} of an ultradispersed rhodium catalyst is characterized by two absorption bands at 2095 and 2027 cm^{-1}. The wave numbers correspond closely to those observed for the bridged $[Rh(CO)_2Cl]_2$ dimer, and are assigned to the symmetrical and antisymmetrical stretching frequencies, respectively. On the basis of these CO infrared data, some investigators have asserted that rhodium on alumina after reduction is monatomically dispersed with the rhodium in the 1+ state [3 - 5].

On the other hand, electron microscopy studies of a well-reduced Rh catalyst showed the existence of metallic rhodium crystallites [6, 7]. The seeming contradiction between the results obtained from infrared studies and those obtained from high resolution electron microscopy is explained by the results of an EXAFS study recently published by van't Blik *et al.* [9, 10]. They observed that after reduction of an ultradispersed catalyst only metallic rhodium crystallites were present, with most likely a three-dimensional structure. After CO admission however, the EXAFS spectrum changed completely. The EXAFS oscillations above $k = 5$ $Å^{-1}$, typical for Rh—Rh metal coordination, had disappeared. The rhodium metallic particles apparently break up on CO adsorption, ultimately leading to isolated rhodium dicarbonyl species. A further analysis of the EXAFS data showed that the oscillations were caused by $O_3Rh^I(CO)_2$ coordination. Each rhodium ion is surrounded by two CO molecules (geminal dicarbonyl) and three oxygen ions of the support. The oxidation state of rhodium changed from zero to 1+ after CO admission; the change was explained in terms of oxidative CO chemisorption via CO dissociation.

These results clearly demonstrate the dramatic influence of CO adsorption at room temperature on the structure of rhodium in highly dispersed catalysts. In general, one must be aware that such effects may occur when these catalysts are studied under different gas atmospheres.

In order to obtain more information about the rhodium structure in a highly dispersed $Rh/\gamma\text{-}Al_2O_3$ catalyst after different treatments, we have carried out an EXAFS *in situ* study of 0.47 and 1.04 wt.% $Rh/\gamma\text{-}Al_2O_3$ catalysts. As we are interested in the hydrogenation of carbon monoxide to hydrocarbons, EXAFS spectra were recorded after reduction with H_2, evacuation, CO admission at room temperature, desorption of CO, CO admission at 523 K (at which temperature the Boudouard reaction takes place ($2CO \rightarrow C + CO_2$)) and after hydrogenation of CO at 523 K. The EXAFS data give insight into the change in local structure of supported rhodium under different conditions.

One of the first EXAFS studies of the effects of adsorption of different gases on the structural and electronic properties of supported metallic

crystallites was reported by Fukushima and Katzer [11], who studied the Pt/Al_2O_3 system and observed that O_2 adsorption caused severe structural disruption of the crystallites, whereas CO adsorption caused only electronic effects.

Experimental

Two $Rh/\gamma\text{-}Al_2O_3$ catalysts were prepared with different rhodium loadings (0.47 and 1.04 wt.%). By pore volume impregnation of the $\gamma\text{-}Al_2O_3$ support (Ketjen, 000-1.5E, specific area = 290 $m^2\ g^{-1}$, pore volume = 0.65 $cm^3\ g^{-1}$) with an aqueous solution of $RhCl_3 \cdot xH_2O$ (39 wt.% Drijfhout) the metal salt was deposited on the support. After impregnation the catalysts were dried at room temperature overnight and subsequently for 16 h at 393 K to remove the adsorbed water. The dried catalysts were directly reduced at 773 K (heating rate 5 K min^{-1}) for 1 h in flowing hydrogen (Research Grade, Hoekloos) and passivated (oxidation at room temperature). The rhodium content of the passivated catalysts was determined colourimetrically.

Temperature-Programmed Reduction (TPR) studies confirmed that after reduction at 773 K, the catalysts were completely reduced. The TPR of the passivated catalysts showed that a temperature of at least 423 K was needed in order to reduce the systems, and moreover that the degree of oxidation of the passivated catalysts was high, although passivation is a mild oxidation. This indicates that the dispersion of the catalysts was high [12].

Hydrogen chemisorption measurements were performed in a conventional glass system at 298 K. Before measuring the H_2 adsorption isotherms, the passivated catalysts were reduced at 573 K (heating rate 5 K min^{-1}) for 1 h under flowing hydrogen, which had been purified by passing over a Pd diffusion cell, and evacuated (10^{-2} Pa) at 573 K for another hour. Following the method of Benson and Boudart [13], the hydrogen chemisorption measurements resulted in H/Rh values (the total amount of chemisorbed H atoms, corrected for adsorption on the bare support, per total amount of rhodium) of 1.7 and 1.6 for the 0.47 and 1.04 wt.% $Rh/\gamma\text{-}Al_2O_3$ catalysts respectively. These results indicate that both catalysts are ultradispersed. H/Rh values higher than 1 for Rh/Al_2O_3 catalysts have been observed previously [14, 15] and are explained by multiple adsorption, although hydrogen spillover cannot be completely excluded [16].

The samples used for the EXAFS experiments were pressed into thin self-supporting wafers and mounted in an EXAFS *in situ* cell [17]. The thickness of the wafer was chosen such that the logarithm of the ratio between the incident and transmitted X-ray intensities approached 1.6. The different treatments of the catalysts were carried out by using Research Grade He, H_2 and CO, which were all purified over a BTS column for the removal of oxygen and over molecular sieves (Union Carbide, 5A) for the removal of water. The EXAFS experiments were carried out on X-ray beam

line I-5 at the Stanford Synchrotron Radiation Laboratory (SSRL) with ring energies of 3 GeV and ring currents of 40 - 80 mA. The EXAFS spectra of the rhodium K-edge were recorded at liquid nitrogen temperature.

The EXAFS data were analyzed by using reference samples with known crystal structure (the theory-independent analysis) and the Fourier filtering approach [18]. As reference compounds we have used Rh foil, powdered Rh_2O_3 and powdered $RhCl_3$. As a suitable reference compound for the rhodium geminal dicarbonyl $Rh(CO)_2$ we have used the dimer $[Rh(CO)_2Cl]_2$, from which the Rh—Cl contribution to the EXAFS data has been subtracted. The procedure for this will be published elsewhere [10]. For a detailed description of the analysis of the EXAFS function, we refer to van Zon *et al.* [19] and van't Blik *et al.* [10]. Before analyzing the EXAFS, the spectra were smoothed by removing high frequency components (noise) in the spectrum via Fourier filtering. The *r*-region from 1 Å to 3.5 Å of the Radial Distribution Function (RDF), in which we are interested, is not affected by the smoothing operation. The Fourier transforms were corrected for phase shift and/or back-scattering amplitude [20]. Consequently the *r* values correspond with real interatomic distances *R* if the phase used for correction originated from the same absorber–scatterer pair as that analyzed.

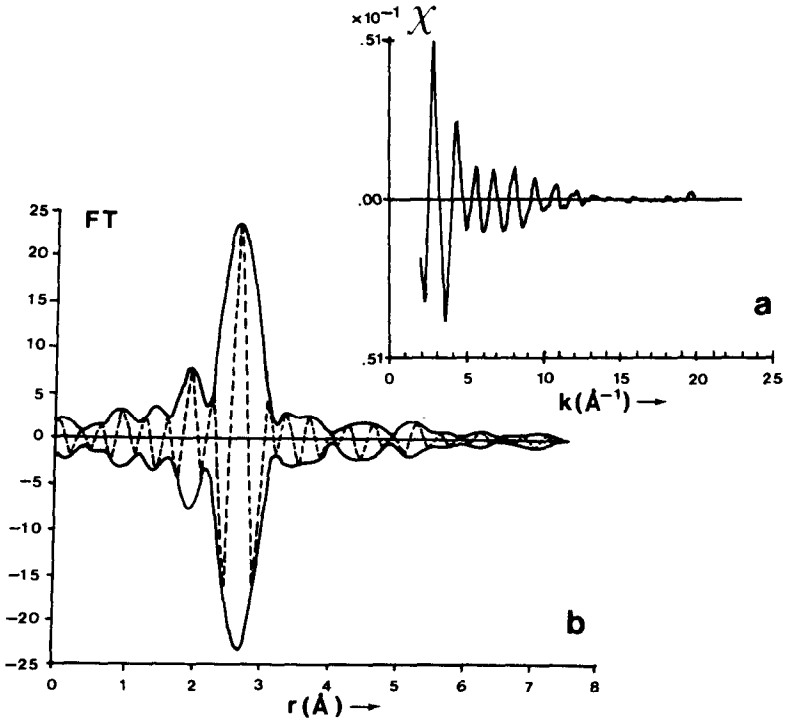

Fig. 1. 0.47 wt.% Rh/γ-Al_2O_3 catalyst after reduction at 673 K: (a) normalized smoothed EXAFS data of the rhodium K-edge at liquid nitrogen temperature; (b) associated k^3-weighed Fourier transform (Δk = 3.3 - 9.9 $Å^{-1}$) corrected for Rh—Rh phase shift and back-scattering amplitude. (——) absolute value |FT''|, (— — —) imaginary part ImFT''.

Results

Reduction at 673 K

Before measuring the EXAFS spectra, both passivated catalysts were reduced in the cell at 673 K for 0.5 h under flowing hydrogen and cooled to room temperature. The smoothed EXAFS function of the rhodium K-edge of the reduced 0.47 wt.% $Rh/\gamma\text{-}Al_2O_3$ catalyst (under 100 kPa H_2, so the crystallites were covered with hydrogen) is given in Fig. 1a. The oscillations are characteristic for rhodium neighbour atoms. Figure 1b shows the imaginary part ImFT'' and the absolute value |FT''| of the k^3-weighed Fourier transform of the smoothed EXAFS data, performed on a k interval from $k = 3.3$ Å^{-1} to $k = 9.9$ Å^{-1} and corrected for Rh—Rh phase shift and Rh—Rh back-scattering amplitude. The EXAFS function of the reduced 1.04 wt.% $Rh/\gamma\text{-}Al_2O_3$ catalyst only differs somewhat in amplitude from that given in Fig. 1a.

Figure 1b clearly shows that the RDF is not symmetrical but is characterized by two peaks, a main peak around $r = 2.7$ Å and a peak around $r = 1.8$ Å. (The procedure for analyzing this type of RDF will be published elsewhere [19].) A careful analysis of the RDF leads to the conclusion that the EXAFS oscillations are a sum of oscillations due to metallic rhodium–rhodium and rhodium–oxygen scatterer pairs [21]. The optimized parameter values R (interatomic distance), N (average coordination number) and $\Delta\sigma^2$ ($= \sigma^2_{\text{catalyst}} - \sigma^2_{\text{reference compound}}$, where σ^2 = thermal and static disorders), determined for the 0.47 and 1.04 wt.% $Rh/\gamma\text{-}Al_2O_3$ catalysts, are presented in Tables 1 and 2 respectively. Figure 2a shows the smoothed EXAFS data with the calculated Rh—Rh, Rh—O two-shell EXAFS function using the optimized parameters (*cf.* Table 1). The associated k^3-weighed Fourier transforms are presented in Fig. 2b.

TABLE 1

EXAFS parameter values for 0.47 wt.% $Rh/\gamma\text{-}Al_2O_3$ catalyst after different treatments

Treatment	Coordination								
	Rh—Rh			Rh—O			Rh—CO		
	N	R (Å)	$\Delta\sigma^2 \times 10^2$ (Å^2)	N	R (Å)	$\Delta\sigma^2 \times 10^2$ (Å^2)	N	R (Å)	$\Delta\sigma^2 \times 10^2$ (Å^2)
A: reduction at 673 K	5.3	2.68	0.5	1.3	2.73	0.0			
B: A, evacuation at 673 K, CO admission at 296 K	1.2	2.68	0.4	2.6	2.10	0.6	1.7 [a]		0.5
C: reduction at 523 K, H_2/CO at 523 K	9.0	2.69	0.3						

[a]The Rh—C and Rh—O* distances are equal to those in the dimer $[Rh(CO)_2Cl]_2$.
Accuracies: N: ±10 - 20%, R: ±0.5 - 1%, $\Delta\sigma^2$: ±10 - 20%.

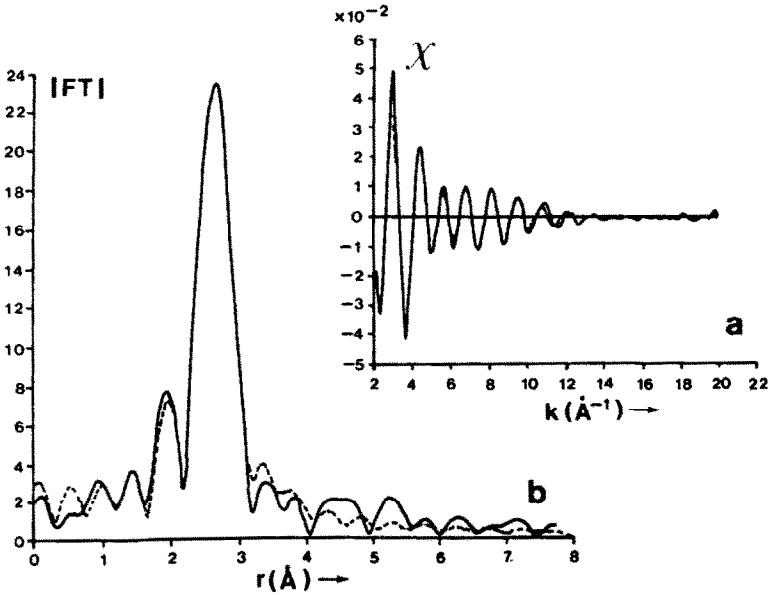

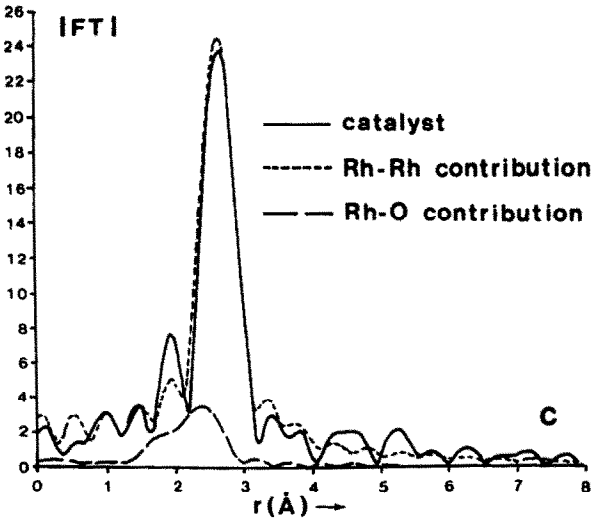

Fig. 2. 0.47 wt.% Rh/γ-Al_2O_3 catalyst after reduction at 673 K: (a) (——) normalized smoothed EXAFS data of the rhodium K-edge at liquid nitrogen temperature, (— — —) obtained by calculating the two-shell EXAFS (Rh—Rh and Rh—O) using the optimized parameters (*cf.* Table 1); (b) associated absolute values of the k^3-weighed Fourier transforms (Δk = 3.3 - 9.9 Å^{-1}) corrected for Rh—Rh phase shift and amplitude; (——) Fourier transform of the catalyst, (— — —) Fourier transform of the calculated Rh—Rh and Rh—O two-shell EXAFS; (c) absolute values of the k^3-weighed Fourier transforms (Δk = 3.3 - 9.9 Å^{-1}) corrected for Rh—Rh phase shift and amplitude for the catalyst and the calculated Rh—Rh and Rh—O one-shell fine structures.

TABLE 2

EXAFS parameter values for 1.04 wt.% $Rh/\gamma\text{-}Al_2O_3$ catalyst after different treatments

Treatment	Coordination								
	Rh—Rh			Rh—O			Rh—CO		
	N	R (Å)	$\Delta\sigma^2 \times 10^2$ (Å^2)	N	R (Å)	$\Delta\sigma^2 \times 10^2$ (Å^2)	N	R (Å)	$\Delta\sigma^2 \times 10^2$ (Å^2)
A: reduction at 673 K	5.9	2.68	0.5	1.1	2.73	0.0			
B: A, evacuation at 673 K	6.6	2.63	0.4						
C: B, CO admission at 296 K	1.6	2.68	0.4	2.2	2.12	0.5	1.5 [a]		0.5
D: C, He flushing at 573 K	7.1	2.66	0.5						
E: D, reduction at 573 K	7.8	2.68	0.4						

[a]The Rh—C and Rh—O* distances are equal to those in the dimer $[Rh(CO)_2Cl]_2$.
Accuracies: N: ±10 - 20%, R: ±0.5 - 1%, $\Delta\sigma^2$: ±10 - 20%.

In order to demonstrate the influence of the Rh—O as well as the Rh—Rh contribution on the Fourier-transformed smoothed EXAFS data, the RDFs of the data, the calculated Rh—Rh one-shell and Rh—O one-shell fine structures are presented in Fig. 2c. Note that the RDF of Rh—O coordination shows a maximum at 2.33 Å, while the real interatomic distance R is 2.73 Å. This is caused by the fact that an Rh—Rh phase shift correction was used. The phase factors of Rh—Rh and Rh—O coordination differ, and in the case of Rh—Rh phase shift correction the r values of Rh—O bonds shift down 0.4 Å relative to the real interatomic distances. The figure clearly demonstrates that the main peak at 2.7 Å is caused by Rh—Rh coordination and is slightly affected by Rh—O coordination, while the apparent peak at 1.8 Å is caused by interference of the two coordinations.

Evacuation at 673 K

A fresh passivated 1.04 wt.% $Rh/\gamma\text{-}Al_2O_3$ sample was reduced at 673 K for 1 h, evacuated (10^{-2} Pa) for another hour and cooled to room temperature under dynamic vacuum. Helium was then admitted up to 100 kPa. Analysis of the EXAFS spectrum of the evacuated catalyst yielded an average Rh—Rh coordination number of 6.6, which is significantly higher than that after reduction without evacuation (N = 5.9), and an interatomic distance of 2.63 ± 0.01 Å indicating a contraction of the metallic rhodium particles (see Table 2). In addition, no substantial contribution of Rh—O coordination could be detected.

CO chemisorption at 296 K

Both catalysts used in the reduction were evacuated (10^{-2} Pa) at 673 K for 1 h and subsequently cooled to room temperature under dynamic

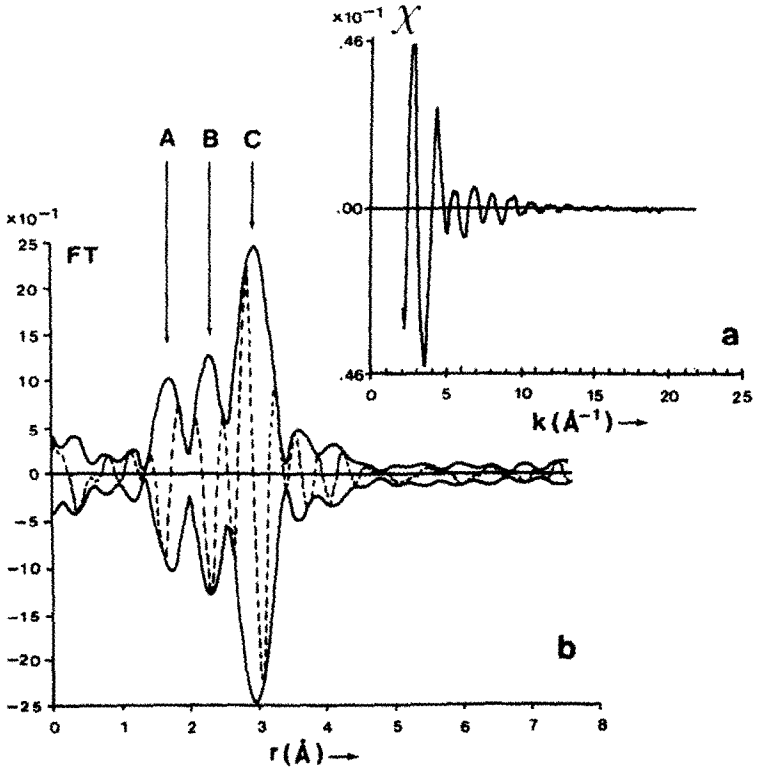

Fig. 3. 0.47 wt.% $Rh/\gamma\text{-}Al_2O_3$ catalyst after CO admission at 296 K: (a) normalized smoothed EXAFS data of the rhodium K-edge at liquid nitrogen temperature; (b) associated k^3-weighed Fourier transform (Δk = 3.3 - 9.7 $Å^{-1}$) corrected for Rh—O phase shift. (——) |FT'|, (— — —) ImFT'.

vacuum. When room temperature was reached, CO was admitted up to 100 kPa, after which the EXAFS spectra were recorded. As the spectra of both catalysts hardly differ, we present in Fig. 3a only the smoothed EXAFS obtained from the 0.47 wt.% $Rh/\gamma\text{-}Al_2O_3$ catalyst. Comparison of the EXAFS after reduction with the EXAFS after CO admission (see respectively Figs. 1a and 3a) clearly demonstrates the diminution of the amplitude after CO adsorption at room temperature. Oscillations above $k = 5$ $Å^{-1}$ typical for rhodium–rhodium coordination are still present. This demonstrates that a partial disruption of the small Rh crystallites has taken place and that a small portion of the rhodium is present as metallic particles, upon which CO is linearly bound, whereas the greater portion is present as isolated $Rh(CO)_2$ species. Both the particles and dicarbonyl species are attached to the support via oxygen ions, but with different interatomic Rh—O distances [10]. As the fraction of the total amount of rhodium involved in the Rh—O bonds between the metallic particles and the support is low, the contribution of this scatterer pair can be neglected. Consequently the EXAFS function is mainly caused by Rh—Rh, Rh—C—O* (actually two scatterer pairs, Rh—C and Rh—O*) and Rh—O coordination, the last of which describes the bond between the $Rh(CO)_2$ species and the support.

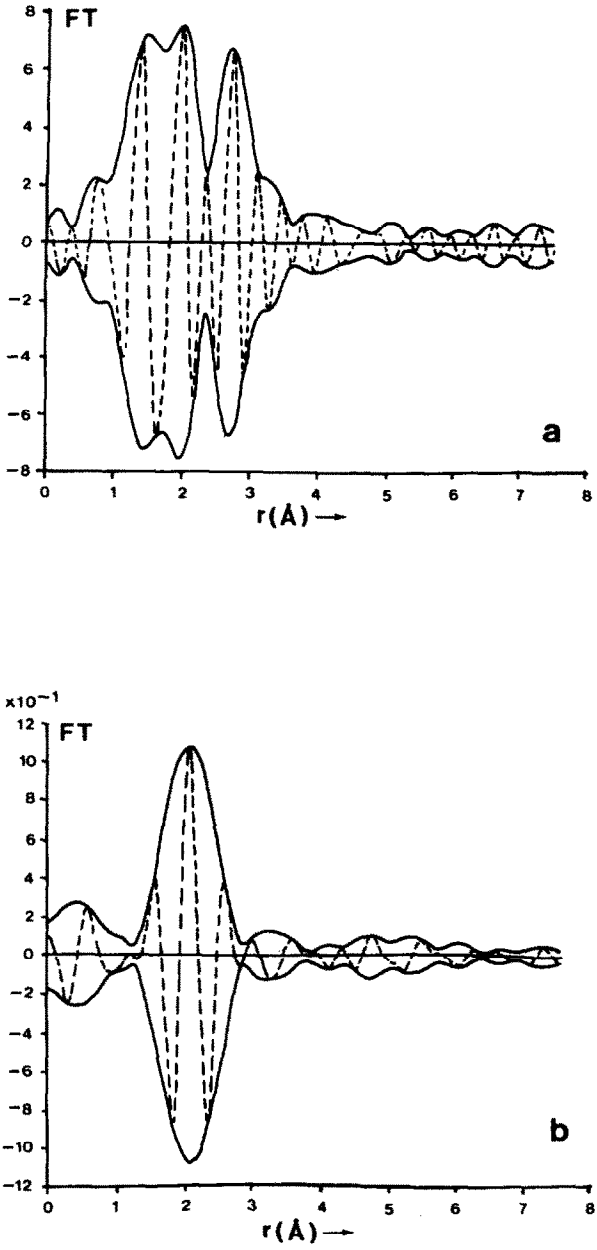

Fig. 4. 0.47 wt.% Rh/γ-Al_2O_3 catalyst after CO admission at 296 K: (a) k^3-weighed Fourier transform (Δk = 3.3 - 10 Å^{-1}) corrected for Rh—Rh phase shift and amplitude of the difference signal between the smoothed data and the calculated Rh—CO contribution using the optimized parameter values (*cf.* Table 1). (——) |FT''|, (— — —) ImFT''; (b) k^3-weighed Fourier transform (Δk = 3.3 - 8.5 Å^{-1}) corrected for Rh—O phase shift of the signal obtained by subtracting the Rh—CO and Rh—Rh contributions from the smoothed EXAFS data using the optimized parameters given in Table 1.

In Fig. 3b the k^3-weighed Fourier transform of the fine structure (Δk = 3.3 - 9.7 Å^{-1}) is given. Three peaks can be distinguished: peak C, which is caused partly by Rh—Rh and partly by Rh—O* coordination; peak A, mainly caused by Rh—C originating from the carbonyl, but may be suppressed by peak B due to interference. As the RDF is corrected for Rh—O phase shift, the r-values which belong to rhodium–oxygen and rhodium–carbon coordination correspond to the real interatomic distances. (The phase factors of Rh—O and Rh—C hardly differ.)

The imaginary part of the Fourier transform between Δr = 1.2 - 1.8 Å can be assigned to Rh—C coordination only. Therefore a first estimate for the Rh—C—O* parameter values was found by calculating the EXAFS of Rh—C—O*, using the phase shift and back-scattering amplitude of the geminal dicarbonyl reference sample, in such a way that the imaginary parts of the transformed calculated EXAFS and the transformed EXAFS data overlap between 1.2 and 1.8 Å. The optimized parameter values (see Table 1) are: N = 1.7, $\Delta\sigma^2$ = 0.005 Å^2 (relative to $[Rh(CO)_2Cl]_2$). The interatomic distances are similar to the Rh—C—O* distances in the dimer.

As mentioned before, peak C in Fig. 3b is caused by Rh—Rh as well as Rh—O* coordination. By subtracting the Rh—C—O* contribution from the EXAFS data, the Rh—Rh contribution can then be determined. Therefore we investigated the difference signal between the smoothed data and the calculated Rh—CO contribution, using the optimized parameter values. The Rh—Rh phase shift and back-scattering amplitude-corrected RDF of this signal is presented in Fig. 4a. In this function two regions can be distinguished: (a) Δr = 1 - 2.2 Å, with relative broad oscillations in ImFT'', typical for Rh—O coordination, (b) Δr = 2.3 - 3.3 Å, with a peak around 2.7 Å, with which the maximum of ImFT'' and |FT''| coincide. The peak belongs to the Rh—Rh nearest neighbour distance, and the optimized Rh—Rh parameter values (see Table 1) were determined by fitting the filtered difference signal, obtained by inverse transformation from r = 2.7 Å to r = 3.7 Å. In order to obtain the Rh—O parameters, the Rh—O phase-corrected RDF of the difference signal between the smoothed EXAFS data and the sum of the calculated Rh—CO and Rh—Rh signals, using the optimized parameters (*cf.* Table 1), was analyzed (see Fig. 4b). A fit of the filtered difference signal (Δr = 1.3 - 2.8 Å) yielded N = 2.6, R = 2.10 Å and $\Delta\sigma^2$ = 0.004 Å^2. Note that ImFT' and |FT'| are symmetric, which is a necessary condition if the EXAFS is due to a single scatterer pair.

Figure 5a shows the smoothed EXAFS data and the calculated three-shell EXAFS function using the parameters given in Table 1. In Fig. 5b and c are respectively the ImFT' and the |FT'| of the associated k^3-weighed Fourier transforms presented. The optimized parameter values determined for the 1.04 wt.% Rh/γ-Al_2O_3 catalyst are presented in Table 2.

CO desorption

As shown above, CO chemisorption at room temperature gave rise to disruption of the rhodium–rhodium bonds. In order to investigate if

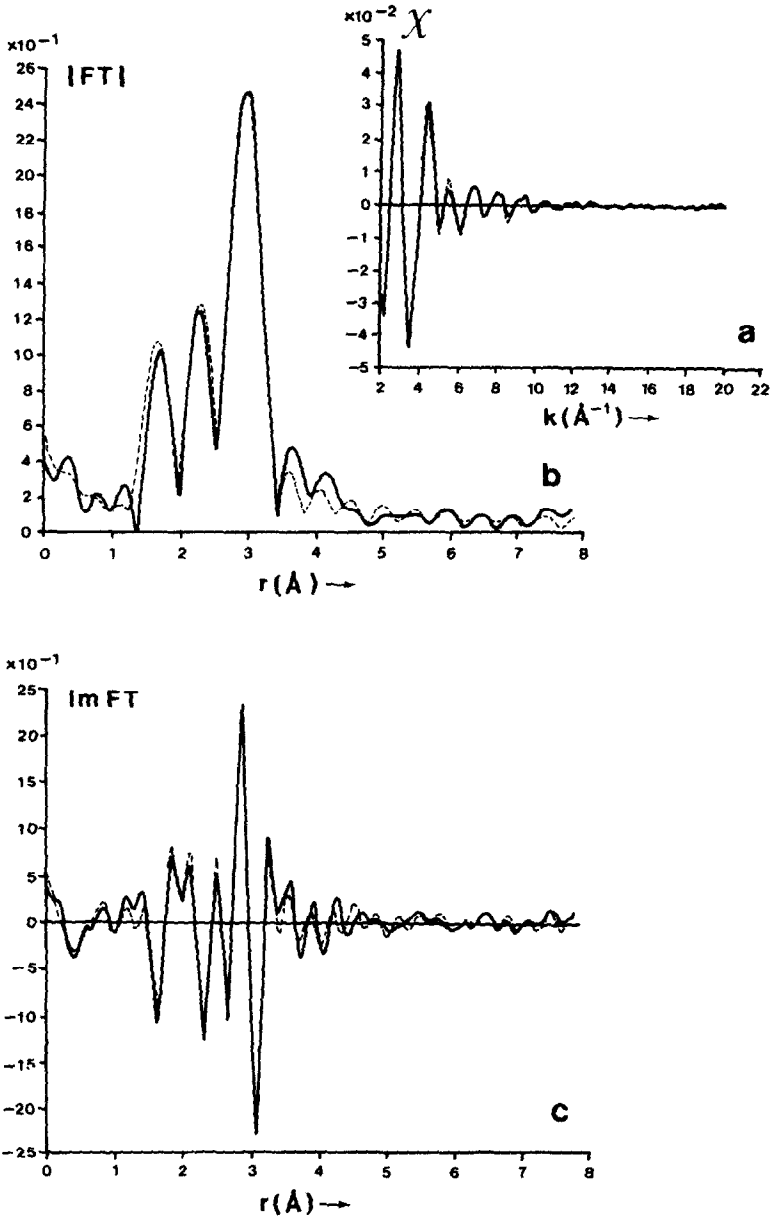

Fig. 5. 0.47 wt.% $Rh/\gamma\text{-}Al_2O_3$ catalyst after CO admission at 296 K: (a) (——) normalized smoothed EXAFS data of the rhodium K-edge at liquid nitrogen temperature, (— — —) calculated Rh—CO, Rh—Rh and Rh—O three-shell EXAFS, using the optimized parameter values (*cf.* Table 1); (b) absolute values of the associated Fourier transforms; (c) imaginary parts of the associated Fourier transforms.

rhodium–rhodium bonds are re-formed after desorption of carbon monoxide, EXAFS spectra of the CO-adsorbed 1.04 wt.% $Rh/\gamma\text{-}Al_2O_3$ catalyst, described above, were recorded after each of the following consecutive

treatments: (a) evacuation (10^{-2} Pa) at room temperature for 5 min and heating at 373 K under flowing He for 1 h; (b) heating at 573 K under flowing He for another hour, and (c) reduction with flowing H_2 at 573 K.

The EXAFS spectrum after flushing with He at 373 K was identical to that obtained after CO admission at room temperature, indicating that no desorption of CO had taken place, while after flushing with He at 573 K the spectrum had completely changed to one typical for rhodium–rhodium nearest neighbours. The optimized parameter values are: $N = 7.1$, $R = 2.66$ Å (a small contraction compared to bulk value) and $\Delta\sigma^2 = 0.0046$ Å^2 (see Table 2). Subsequent reduction at 573 K caused an enhancement of the average Rh—Rh coordination number from $N = 7.1$ to $N = 7.8$, while the interatomic distance increased to the bulk value (see Table 2).

Boudouard reaction and reaction between H_2 and CO

After the EXAFS spectrum of the 0.47 wt.% Rh/γ-Al_2O_3 catalyst adsorbed with CO was recorded (see above), the temperature was raised to 523 K under flowing CO. Under these conditions the Boudouard reaction takes place, as confirmed by CO-pulse experiments. From the EXAFS results we can safely say that a contribution from Rh—Rh coordination is lacking. The EXAFS is very complicated, and could not be analyzed properly because too many scatterers of different types contribute (Rh—C from

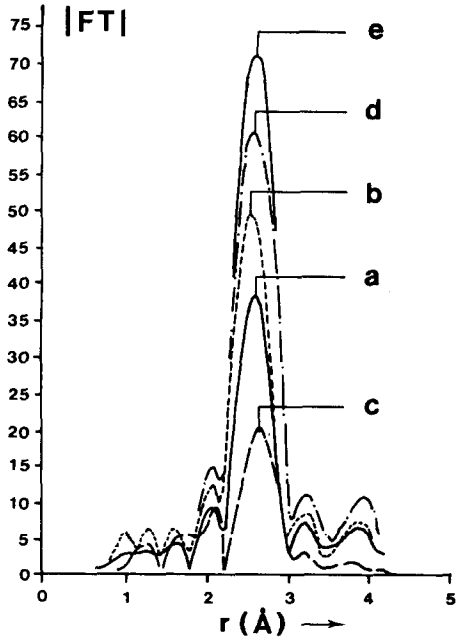

Fig. 6. RDFs (k^3-weighed, $\Delta k = 3 - 13$ Å^{-1}, Rh—Rh phase shift and amplitude-corrected) for the 1.04 wt.% Rh/γ-Al_2O_3 catalyst after the consecutive treatments: (a) reduction at 673 K, (b) evacuation at 673 K, (c) CO admission at 296 K, (d) He flushing at 573 K and (e) reduction at 573 K.

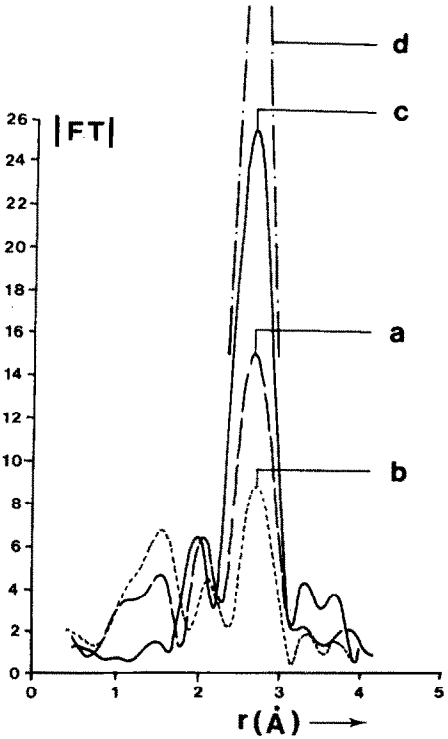

Fig. 7. RDFs (k^3-weighed, Δk = 3.3 - 10 $Å^{-1}$, Rh—Rh phase shift and amplitude-corrected) for the 0.47 wt.% Rh/γ-Al_2O_3 catalyst after the consecutive treatments: (a) reduction at 673 K, (b) CO admission at 296 K and (c) Boudouard reaction at 523 K; (d) reduction of the passivated catalyst at 523 K and subsequent reaction between H_2 and CO at 523 K.

rhodium carbonyl and possible formed rhodium carbide, Rh—O* from rhodium carbonyl and Rh—O from the interface support/rhodium species and rhodium oxide, formed by intercalation of oxygen atoms during the Boudouard reaction).

A passivated 0.47 wt.% Rh/γ-Al_2O_3 sample was reduced at 523 K for 15 min and subsequently a mixture of H_2 and CO (1:1) was led over the catalyst for 1 h. Under these conditions hydrocarbons are formed.

The EXAFS spectrum obtained after reaction showed oscillations due to rhodium–rhodium coordination only. By fitting the filtered RDF in the k-space, the parameters of the rhodium nearest-neighbour shell were determined: N = 9.0, R = 2.69 Å, $\Delta\sigma^2$ = 0.003 $Å^2$ (see Table 1).

The results of the influence of different gas environments upon the Rh—Rh nearest neighbour coordination are summarized in Figs. 6 and 7. In Fig. 6, the Rh—Rh phase and amplitude-corrected RDFs of the EXAFS spectra obtained from the 1.04 wt.% Rh/γ-Al_2O_3 catalyst after different treatments are presented. This figure illustrates the disruption of Rh—Rh bonds caused by CO chemisorption and rearrangement of the metal cluster

after desorption of CO. The alteration of the structure of the rhodium crystallites after the Boudouard reaction and hydrogenation of carbon monoxide are shown in Fig. 7. The different RDFs of the fine structures measured on the 0.47 wt.% $Rh/\gamma\text{-}Al_2O_3$ catalyst are depicted.

Discussion

The EXAFS results clearly indicate that the structure of rhodium in a highly dispersed Rh/Al_2O_3 catalyst changes significantly when the gas atmosphere is altered.

After reduction of the catalysts, rhodium crystallites were formed having an interatomic rhodium–rhodium distance of 2.68 Å which approached the bulk value (2.687 Å) within experimental error (0.01 Å). The structure of the crystallites after reduction can be either two-dimensional, as suggested by Yates *et al.* [6], or three-dimensional, as suggested by van't Blik *et al.* [10]. Assuming a square two-dimensional particle with a (111) fcc surface, the particle with an average coordination number of 5.3 (observed for the reduced 0.47 wt.% $Rh/\gamma\text{-}Al_2O_3$ catalyst) consists of approximately 120 atoms, which corresponds to a diameter of the raft of 20 Å. If the H/Rh_s stoichiometry of edge and corner atoms is 2 (1 for the other atoms), as proposed by Yates *et al.* [6], the H/Rh value would be about 1.3. This value is too different from the experimental value of 1.7, so the metallic particles most likely have a three-dimensional structure. Assuming that these particles have an fcc structure, the average coordination number of 5.3 corresponds with crystallites of approximately 13 atoms (3 atoms in the first layer, 7 atoms in the second layer and 3 atoms in the third layer) of which 12 atoms have been exposed. The observed H/Rh value of 1.7 can be understood if the H/Rh_s stoichiometry is 2.

Evidence was found for Rh—O coordination. The interatomic distance of 2.73 Å is 0.68 Å larger than the distance in Rh_2O_3, indicating that the rhodium crystallite is attached to the support via an interaction between zero-valent rhodium atoms and oxygen ions of the $\gamma\text{-}Al_2O_3$. This result has previously been reported by van Zon *et al.* [21].

After evacuation of the 1.04 wt.% $Rh/\gamma\text{-}Al_2O_3$ catalyst, the rhodium–rhodium bond was shortened by 0.05 Å (see Table 2), which is far beyond experimental error. As nearly all the atoms are situated on the surface, the observed contraction is in accordance with the prediction of Allen [22] that a contraction of distances between atoms of a surface layer occurs with an enhancement of the force constants. A contraction of small metal crystallites covered with helium has been observed previously by Moraweck *et al.* [23] who found a contraction of 0.12 Å of the Pt—Pt distance in a Pt/Y-zeolite sample.

As can be seen from Table 2, evacuation causes not only a decrease in the Rh—Rh distance but also an increase in the average coordination number. In our case, a change of N from 5.9 to 6.6 occurs after evacuation and

He flushing. Normal sintering of the crystallites cannot be excluded, but the increase can also be interpreted in terms of a 'breathing' crystallite [7]. The crystallites which are covered with hydrogen are spread over the support. After desorption of hydrogen the surface atoms become (more) coordinatively unsaturated, and consequently the particles curl up to form crystallites with the smallest possible number of surface atoms. Unfortunately we have not recorded an EXAFS spectrum after a subsequent H_2 admission at room temperature in order to prove this hypothesis.

The EXAFS results clearly show that the majority of rhodium–rhodium bonds are broken upon CO chemisorption, ultimately leading to rhodium geminal dicarbonyl species as shown previously [9, 10]. In addition to isolated $Rh(CO)_2$ species, crystallites are still present. During reduction of the catalyst, particles of different sizes are formed; the crystallites with a large average rhodium–rhodium coordination number are not broken up after CO adsorption because the adsorption energy provided is too low to disrupt all the rhodium–rhodium bonds. Note that the measured coordination numbers as given in Tables 1 and 2 are expressed per absorbing Rh atom. The actual average coordination number of a species can be found by dividing the measured one with the fractional part of the total number of rhodium atoms in the species in question. An approximation of the real average rhodium–rhodium coordination number of the crystallites which were not affected during CO chemisorption can be given. The real coordination number of rhodium geminal dicarbonyl species is 2. In the case of the 1.04 wt.% $Rh/\gamma\text{-}Al_2O_3$ catalyst, the determined N(Rh—CO) is 1.5 (*cf.* Table 2). The Rh—O* and Rh—C contributions to the EXAFS function of linearly bound carbon monoxide on the surface rhodium atoms of the crystallites remaining after CO adsorption can be neglected because the relative contribution to Rh—CO oscillations is less than 5%. The fraction f of the total number of rhodium atoms in the $Rh(CO)_2$ species is $1.5/2 = 0.75$. It is now also possible to estimate the real average coordination number of the crystallites, which is $N(\text{Rh—Rh})/(1 - f) = 6.4$.

Evidence has been found for Rh—O coordination with an interatomic distance of 2.10 Å, which is 0.05 Å longer than the distance in Rh_2O_3 and 0.63 Å shorter than the Rh—O distance observed after reduction of the catalyst. As previously published [10], the Rh—O distance of 2.10 Å is attributed to the bond between the $Rh^I(CO)_2$ species and the support. The oxidation state of rhodium changes from zero to 1+ during CO admission and is interpreted as being due to dissociation of carbon monoxide. The ratio N(Rh—O)/N(Rh—CO) for both catalysts is about 1.5, which indicates that on the average each $Rh(CO)_2$ species is bound to the support by three oxygen ions.

The stability of the $Rh^I(CO)_2$ species is substantial, as illustrated by the EXAFS spectrum which remained constant after He flushing at 373 K. A striking feature of the catalyst is the rearrangement of the metal clusters after desorption of carbon monoxide at elevated temperature (573 K). This indicates that the disruption and rearrangement of the metallic rhodium

particles is a reversible process, and that the adsorption and desorption of carbon monoxide are oxidative and reductive respectively. As proposed elsewhere [10], reduction of the rhodium takes place via oxidation of CO to CO_2, and increases the size of the formed crystallites. The average coordination number of the particles in the catalyst after CO desorption (N(Rh—Rh) = 7.1) is significantly higher than in the evacuated catalyst (N(Rh—Rh) = 6.6). In agreement herewith, the contraction of the rhodium–rhodium bond (R = 2.66 Å) is less pronounced than the distance in the particles in the reduced and evacuated catalyst (R = 2.63 Å). A subsequent reduction results in an increase in the average Rh—Rh coordination number. The crystallites are covered with hydrogen and a relaxation of the rhodium–rhodium distance occurs (R = 2.68 Å). A decrease in the dispersion of a highly dispersed Rh/Al_2O_3 catalyst after CO adsorption and subsequent reduction has also been observed by Yates *et al.* [6].

After CO flushing at 523 K, at which temperature the Boudouard reaction takes place, the rhodium particles break up completely, probably due to intercalation of carbon and/or oxygen atoms. The peak around 2.8 Å in the RDF (see Fig. 7) belongs to the Rh—O distance originating from carbon monoxide either bridged or linearly bonded to rhodium.

During the hydrogenation of carbon monoxide, a substantial sintering of the highly dispersed 0.47 wt.% Rh/γ-Al_2O_3 catalyst occurred. The average coordination number changed from N(Rh—Rh) = 5.3 to 9.0 which corresponds with metallic particles consisting of about 20 and 200 atoms respectively. This result clearly illustrates that under reaction conditions the advantages of having a highly dispersed system can be nullified.

Conclusions

The EXAFS experiments clearly illustrate a substantial alteration of the topology of rhodium in highly dispersed Rh/Al_2O_3 catalysts after different treatments.

During reduction small metallic rhodium particles are formed, and when covered with hydrogen, the Rh—Rh interatomic distance is 2.68 Å, which is similar to that in the Rh foil. The crystallites are attached to the support via rhodium–oxygen bonds with a length of 2.73 Å, which is 0.68 Å longer than the Rh—O distance in Rh_2O_3. This indicates that at the crystallite/support interface only zero-valent rhodium is present.

When metallic particles are covered with helium, a contraction of the rhodium–rhodium bond occurs and the average coordination number increases.

CO adsorption at room temperature is oxidative and induces a disruption of rhodium–rhodium bonds, ultimately leading to $O_3Rh^I(CO)_2$ species. The rhodium bonds in particles with a notable size are not affected.

The crystallites which are broken up due to CO chemisorption are rearranged again after CO is desorbed. The CO desorption occurs via a

reductive reaction, inferred because the valence of rhodium changes from 1+ to zero during evacuation.

After the Boudouard reaction at 523 K ($2CO \rightarrow C + CO_2$) the rhodium–rhodium bond has disappeared, probably because of intercalation of carbon and/or oxygen atoms.

During reaction between CO and H_2 at 523 K, the highly dispersed catalyst is transformed into a poorly dispersed system due to sintering of the metallic crystallites.

Acknowledgements

This work was done at SSRL (Stanford University), which is supported by the NSF through the Division of Materials Research and by the NIH through the Biotechnology Resource Program in the Division of Research Resources, in cooperation with the Department of Energy. We gratefully acknowledge the assistance of the SSRL staff and thank Dr. D. E. Sayers for fruitful discussions.

This study was supported by the Netherlands Foundation for Chemical Research (SON) with financial aid from the Netherlands Organization for the Advancement of Pure Research (ZWO). One of us (D.C.K.) would like to thank ZWO also for supplying a travel grant (R71-34).

References

1 (a) P. R. Watson and G. A. Somorjai, *J. Catal.*, *72* (1981) 347; (b) P. R. Watson and G. A. Somorjai, *J. Catal.*, *74* (1982) 282.
2 T. P. Wilson, P. H. Kasai and P. C. Ellgen, *J. Catal.*, *69* (1981) 193.
3 C. A. Rice, S. D. Worley, C. W. Curtis, J. A. Guin and A. R. Tarrer, *J. Chem. Phys.*, *74* (1981) 6487.
4 R. R. Cavanagh and J. T. Yates, *J. Chem. Phys.*, *74* (1981) 4150.
5 M. Primet, *J. Chem. Soc., Faraday Trans. I*, *74* (1978) 2570.
6 D. J. C. Yates, L. L. Murrell and E. B. Prestridge, *J. Catal.*, *57* (1979) 41.
7 D. J. C. Yates, L. L. Murrell and E. B. Prestridge, in J. Bourdon (ed.), *Growth and Properties of Metal Clusters*, Elsevier, Amsterdam, 1980, p. 137.
8 F. W. Graydon and M. D. Langan, *J. Catal.*, *69* (1981) 180.
9 H. F. J. van't Blik, J. B. A. D. van Zon, T. Huizinga, J. C. Vis, D. C. Koningsberger and R. Prins, *J. Phys. Chem.*, *87* (1983) 2264.
10 H. F. J. van't Blik, J. B. A. D. van Zon, T. Huizinga, J. C. Vis, D. C. Koningsberger and R. Prins, *J. Am. Chem. Soc.*, submitted for publication.
11 T. Fukushima and J. R. Katzer, *Int. Congr. Catal.*, Tokyo, 1980.
12 J. C. Vis, H. F. J. van't Blik, T. Huizinga, J. van Grondelle and R. Prins, *J. Mol. Catal.*, *25* (1984) 367.
13 J. E. Benson and M. Boudart, *J. Catal.*, *4* (1965) 704.
14 H. C. Yao, S. Japar and M. Shelef, *J. Catal.*, *50* (1977) 407.
15 S. E. Wanke and N. A. Dougharty, *J. Catal.*, *24* (1972) 367.
16 R. R. Cavanagh and J. T. Yates, Jr., *J. Catal.*, *68* (1981) 22.
17 D. C. Koningsberger and J. W. Cook, in A. Bianconi, L. Incoccia and S. Stipcich (eds.), *EXAFS and Near-edge Structures*, Springer, Berlin, 1983, p. 412.

18 E. A. Stern, D. E. Sayers and F. W. Lytle, *Phys. Rev., B11* (1975) 4836.
19 J. B. A. D. van Zon, D. C. Koningsberger, H. F. J. van't Blik and D. E. Sayers, *J. Chem. Phys.*, to be published.
20 P. A. Lee and G. Beni, *Phys. Rev., B15* (1977) 2862.
21 J. B. A. D. van Zon, D. C. Koningsberger, D. E. Sayers, H. F. J. van't Blik and R. Prins, *J. Chem. Phys., 80* (1984).
22 G. Allen, *Surf. Sci., 89* (1979) 142.
23 B. Moraweck, G. Clugnet and A. J. Renouprez, *Surf. Sci., 81* (1979) L631.